Optimization of nonlinear error for weighted essentially non-oscillatory methods in direct numerical simulations of compressible turbulence

Ellen M. Taylor, Minwei Wu, M. Pino Martín *

Department of Mechanical and Aerospace Engineering, Princeton University, Princeton, NJ 08544, United States

Abstract

Weighted essentially non-oscillatory (WENO) methods have been developed to simultaneously provide robust shock-capturing in compressible fluid flow and avoid excessive damping of fine-scale flow features such as turbulence. Under certain conditions in compressible turbulence, however, numerical dissipation remains unacceptably high even after optimization of the linear component that dominates in smooth regions. We therefore construct and evaluate WENO schemes that also reduce dissipation due to one source of *non*linear error: the smoothness measurement that governs the application of stencil adaptation away from the linear optimal stencil. Direct numerical simulations (DNS) include a one-dimensional Euler solution and three-dimensional compressible isotropic turbulence. We find that the smoothness measurement modifications that we call the ''relative smoothness limiter'' and the ''relative total variation limiter'' each significantly enhance thez grid-convergence properties of WENO schemes while generating, respectively, small and moderate additional computational expense. Moreover, we observe these techniques to be broadly effective regardless of flow configuration.
© 2006 Elsevier Inc. All rights reserved.

Keywords: Direct numerical simulation; Compressible turbulence; Shock capturing; Numerical dissipation; Non-linear dissipation; Limiters; Linear dissipation

1. Introduction

The detailed simulation of compressible turbulence requires numerical methods that simultaneously avoid excessive damping of spatial features over a large range of length scales and prevent spurious oscillations near shocks and shocklets (small transient shocks) through robust shock-capturing. Numerical schemes that were developed to satisfy these constraints include, among others, weighted essentially non-oscillatory (WENO) methods [1]. WENO schemes compute numerical fluxes using several different candidate stencils and form a final flux approximation by summing weighted contributions from each stencil. Smoothness measurements

cause stencils that span large flow field gradients to be assigned small relative weights so that a nearly discontinuous shock would provide a weight of almost zero to any stencil containing it. In smooth regions, the relative values of the weights are designed to be optimal by some gauge such as maximum order of accuracy or maximum bandwidth-resolving efficiency.

Jiang and Shu [2] cast the WENO methodology into finite-difference form and provide an efficient implementation of robust and high-order-accurate WENO schemes. Unfortunately, these schemes often generate excessive numerical dissipation for detailed simulations of turbulence, especially for large-eddy simulations (LES) [3]. WENO dissipation arises from two distinct sources: (i) the optimal stencil, which on its own describes a linear scheme, and (ii) the adaptation mechanism, which drives the final numerical stencil away from the optimal one. Bandwidth optimization can reduce the dissipation of the optimal stencil [4,5]; and Martín et al. [5] demonstrate that such a bandwidth-optimized symmetric WENO method indeed reduces numerical dissipation and provides accurate results for direct numerical simulations (DNS) of isotropic turbulence and turbulent boundary layers.

Nonetheless, engaging the nonlinear WENO adaptation mechanism still causes significant local dissipation that can negatively affect global flow properties. Though higher resolution compensates for this, in some cases adequately increasing the number of grid points is not feasible. According to Martín [6], even linearly optimized WENO schemes fail during LES of turbulent boundary layers because of insufficient distinction between shock-containing and smooth regions on typical LES grids. Additionally, Wu et al. [7] have encountered disparities between DNS and experiments of shock/turbulent-boundary-layer interactions and have determined that nonlinear WENO dissipation is responsible for the disagreement even at the highest possible resolutions. There are two primary sources of nonlinear error: (i) the smoothness measurement that governs the application of WENO stencil adaptation and (ii) the coefficients of the individual candidate stencils that govern numerical accuracy when adaptation engages. We will address the first. Previous work in this particular area includes that of Wang and Chen [8], who have examined upwind-biased WENO methods in linearized problems, and Henrick et al. [9], who have examined upwind-biased WENO methods in linear and nonlinear problems. Neither has considered fully turbulent flow fields.

The purpose of this paper is to construct and evaluate linearly optimized WENO schemes that also reduce dissipation due to the nonlinear error arising from the WENO smoothness measurement for DNS of compressible turbulence. Section 2 briefly describes the WENO methodology. In Section 3, we present the motivation for and derivation of two related techniques that overwrite smoothness measurement values with limiting values under certain conditions in order to impede over-adaptation tendencies. Section 4 then demonstrates the effects of these techniques on numerical simulations of a pseudoturbulent flow, the Shu–Osher problem, and a fully turbulent flow, compressible isotropic turbulence. Conclusions are drawn in Section 5.

2. WENO Methodology

We describe the symmetric WENO methodology [4,5] in the context of the one-dimensional advection equation,

$$\frac{\partial u}{\partial t} + \frac{\partial}{\partial x} f(u) = 0 \tag{1}$$

This model equation represents the decoupled forms of equations belonging to any system of hyperbolic conservation laws after a transformation from physical into characteristic space. If the spatial domain is discretized such that $x_i = i\Delta$, in which Δ is the grid spacing, and $u_i = u(x_i)$, Eq. (1) may be cast into the semidiscretized form

$$\frac{\mathrm{d}u_i}{\mathrm{d}t} = -\frac{1}{\Delta}\left(\hat{f}_{i+\frac{1}{2}} - \hat{f}_{i-\frac{1}{2}}\right) \tag{2}$$

in which $\hat{f}_{i+1/2}$ is a numerical approximation of $f(u(x_{i+1/2}))$. Once the right-hand side of this expression has been evaluated, numerical techniques for solving ordinary differential equations, such as Runge–Kutta methods, may be employed to advance the solution in time. In order to ensure stability, procedures that approximate $f(u)$ split it into $f^+(u)$, which has a strictly non-negative derivative, and $f^-(u)$, which has a strictly non-positive one.

WENO schemes compute $\hat{f}^{+}_{i+1/2}$ through reconstructed interpolating polynomials on a number of candidate stencils each containing r grid points. In the symmetric WENO method, there are $(r+1)$ stencils in total. The one fully upwinded stencil ranges from $(i-r+1)$ to i, the one fully downwinded stencil ranges from $(i+1)$ to $(i+r)$, and the other stencils fall in between these two extremes. Fig. 1 provides a schematic of this arrangement for $r = 3$. Throughout this paper, we will abbreviate any WENO implementation in which the candidate stencils contain r points as "WENO-r."

If the flux approximation on stencil k, which contains r grid points, is designated q^{r}_{k} and the weight assigned to that stencil is ω_k, the final numerical approximation becomes

$$\hat{f}^{+}_{i+\frac{1}{2}} = \sum_{k=0}^{r} \omega_k q^{r}_{k} \tag{3}$$

Specifically, q^{r}_{k} emerge from reconstructed polynomial interpolants of maximal order r and are defined as

$$q^{r}_{k}\big|_{i+\frac{1}{2}} = \sum_{l=0}^{r-1} a^{r}_{kl} f(u_{i-r+k+l+1}) \tag{4}$$

in which a^{r}_{kl} are tabulated coefficients; and ω_k are normalized forms of weights Ω_k defined as

$$\Omega_k = \frac{C^{r}_{k}}{(\varepsilon + \mathrm{IS}_k)^p} \tag{5}$$

in which ε prevents division by zero, IS_k is a smoothness measurement that becomes large when discontinuities are present within stencil k, and p may be varied to increase or decrease WENO adaptation sensitivity. $p = 1$ typically provides sufficient adaptation with minimal dissipation. In completely smooth regions, each stencil is equally desirable, and ω_k revert to the optimal weights C_k. As formulated by Jiang and Shu [2],

$$\mathrm{IS}_k = \sum_{m=1}^{r-1} \Delta^{2m-1} \int_{x_{i-1/2}}^{x_{i+1/2}} \left[\frac{\partial^m}{\partial x^m} q^{r}_{k}(x) \right]^2 \mathrm{d}x \tag{6}$$

in which $q^{r}_{k}(x)$ is a reconstructed interpolating polynomial for the flux that may or may not be the same as the one that leads to $q^{r}_{k}|_{i+1/2}$. in Eq. (4). Equivalently,

$$\mathrm{IS}_k = \sum_{l=0}^{r-1} \sum_{m=0}^{r-1} d^{r}_{klm} f(u_{i-r+k+l+1}) f(u_{i-r+k+m+1}) \tag{7}$$

in which d^{r}_{klm} are the coefficients that arise from Eq. (6).

The corresponding stencil diagram for $\hat{f}^{-}_{i+1/2}$ is simply a mirror image of Fig. 1. Because the total number of data points available to the symmetric WENO algorithm is $2r$, its maximum order of accuracy is also $2r$; however, the optimal stencils employed in the current work are bandwidth-optimized [4,5] such that only rth-order accuracy can be guaranteed. The bandwidth-optimization process also introduces a small amount of artificial dissipation to an otherwise neutrally stable optimal stencil to enhance its stability. In practice, the weight of the fully downwinded stencil ω_r is artificially constrained to be no greater than the least of the others so that other adverse stability effects are avoided.

The continuity of the WENO weighting process allows the performance characteristics of the final numerical stencil to theoretically fall anywhere between those of the least favorable candidate stencil and those of the
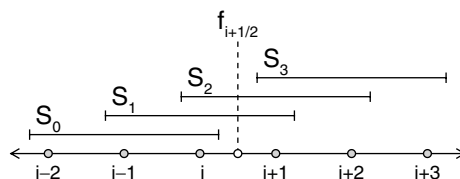

Fig. 1. Symmetric WENO candidate stencils for approximating the numerical flux $\hat{f}^{+}_{i+1/2}$ when the number of points per candidate stencil is $r = 3$.

optimal stencil. In order to gauge this variation quantitatively but efficiently in a flow field, Weirs [4] proposed a combination of the adaptive stencil weights called the nonlinearity index (NI). It is essentially a measure of the degree of departure from the optimal stencil and is defined as

$$\text{NI} = \left(\sum_{k=0}^{r} \left[1 - \frac{(r+1)(\Omega_k/C_k)}{\sum_{l=0}^{r}(\Omega_l/C_l)} \right]^2 \right)^{\frac{1}{2}} \tag{8}$$

This definition forces NI to always be non-negative, and only the optimal stencil can provide a value of zero. It reaches its theoretical maximum, which is $\sqrt{r(r+1)}$, when any one candidate stencil is chosen exclusively. We will often report NI in terms of NI′, its value normalized by this maximum. Ideally, in smooth regions where WENO adaptation is unnecessary, NI′ ≪ 1 so that the favorable performance capabilities of the optimal stencil are realized.

3. Relative limiters

Because the optimal stencil of a WENO scheme provides optimal performance in smooth regions, any technique that discourages unnecessary adaptation can improve WENO dissipation characteristics in compressible turbulence. This approach requires modification of the smoothness measurement but does *not* affect the candidate stencil coefficients a_{kl} in Eq. (4) or the optimal stencil weights.

When the reconstructed polynomial interpolant $q_k^r(x)$ in Eq. (6) is order-optimized (i.e. replicates tabulated data exactly), the Taylor expansion of IS_k yields

$$\text{IS}_k = \Delta^2 [f'(u_i)]^2 + \text{O}(\Delta^4) \tag{9}$$

Ideally, in smooth regions where WENO adaptation is unnecessary, IS_k should be of the order of ε from Eq. (5); in other words, $\text{IS}_k \ll 1$. Now consider a linearly advected smooth sinusoidal function of nondimensional wavenumber κ (nondimensionalized by Δ):

$$f(u(x)) = u(x) = \sin\left(\frac{\kappa x}{\Delta}\right) \tag{10}$$

In this case, Eq. (9) becomes

$$\text{IS}_k(x) = \kappa^2 \cos^2\left(\frac{\kappa x}{\Delta}\right) + \text{O}(\Delta^4) \tag{11}$$

Thus for smoothly varying functions, $\text{IS}_k < 1$ requires $\kappa < 1$, which corresponds to a grid resolution of more than roughly six grid points per wavelength (PPW). To ensure that $\text{IS}_k < 0.1$ more than 20 points per wavelength are necessary. These restrictions indicate that the WENO smoothness measurement as defined in Eq. (6) triggers adaptation too readily and thereby causes unnecessarily degradation of WENO performance.

Jiang and Shu [2] suggest that the over-adaptation tendencies of WENO methods may be mitigated by redefining the smoothness measurement IS_k at points where it falls below a threshold value.

$$\text{IS}_k = \begin{cases} 0, & \text{IS}_k < \alpha_{\text{AL}} \\ \text{IS}_k, & \text{otherwise} \end{cases} \tag{12}$$

In this procedure, effectual values of the absolute smoothness limiter α_{AL} are arbitrary and strongly depend on the specific flow field configuration. Because it is preferable to achieve wide applicability to general turbulent flows, we propose a modified limiting procedure:

$$\text{IS}_k = \begin{cases} 0, & R(\text{IS}) < \alpha_{\text{RL}} \\ \text{IS}_k, & \text{otherwise} \end{cases} \tag{13}$$

in which

$$R(\mathrm{IS}) = \frac{\max_{0 \leq k \leq r} \mathrm{IS}_k}{\varepsilon + \min_{0 \leq k \leq r} \mathrm{IS}_k} \tag{14}$$

and in turn ε is the value employed in Eq. (5). Though the relative smoothness limiter α_{RL} is still arbitrary, the focus on relative rather than absolute thresholds allows a general effectual value to be obtained. Fig. 2 displays the WENO-3 and WENO-4 methods' $R(\mathrm{IS})$ for the sinusoidal wave described above on grids providing six, eight, and twelve points per wavelength. It is apparent that for six or more points per wavelength, $R(\mathrm{IS})$ is less than approximately one order of magnitude, and therefore we set $\alpha_{\mathrm{RL}} = 10$ in Eq. (13). Any WENO method that employs the relative smoothness limiting procedure with this threshold value will be referred to as WENO-RL.

Redefining the smoothness measurement IS_k in the manner of Eq. (13) is not necessarily restricted to information contained within the smoothness measurement itself. Though the smoothness values of the various candidate stencils are already present within the WENO methodology and are therefore convenient, the decision to forcibly apply the optimal stencil can also derive from other criteria. We consider in particular the total variation (TV) of the flux $f(u)$ from Eq. (1) over each candidate stencil. This variation is defined as
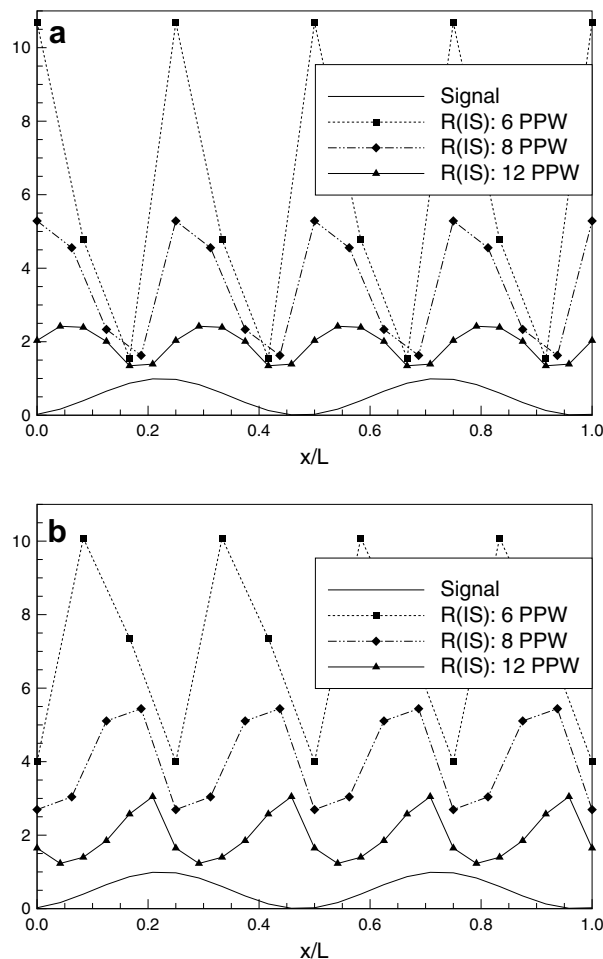

Fig. 2. (a) WENO-3. (b) WENO-4. Ratio of maximum to minimum WENO smoothness measurement IS_k for a smooth sinusoidal function on grids providing varying points per wavelength (PPW).

$$TV_k = \sum_{l=1}^{r-1} |f(u_{i-r+k+l+1}) - f(u_{i-r+k+l})| \tag{15}$$

With this, we can construct a total variation analog to Eq. (14), which is

$$R(TV) = \frac{\max_{0 \le k \le r} TV_k}{\varepsilon + \min_{0 \le k \le r} TV_k} \tag{16}$$

and, in turn, an analog to Eq. (13), which is

$$IS_k = \begin{cases} 0, & R(TV) < \alpha_{RL}^{TV} \\ IS_k, & \text{otherwise} \end{cases} \tag{17}$$

Note that in regions where the optimal stencil has *not* been forcibly imposed by this procedure, the smoothness measurement IS_k still governs WENO adaptation. Fig. 3 shows the WENO-3 and WENO-4 methods' $R(TV)$ for the same sinusoidal wave as in Fig. 2, and upon observing that smooth variations may produce ratios of as much as 5:1, we set $\alpha_{RL}^{TV} = 5$ in Eq. (17). Any WENO method that employs the relative total variation limiting procedure with this threshold value will be referred to as WENO-RLTV.
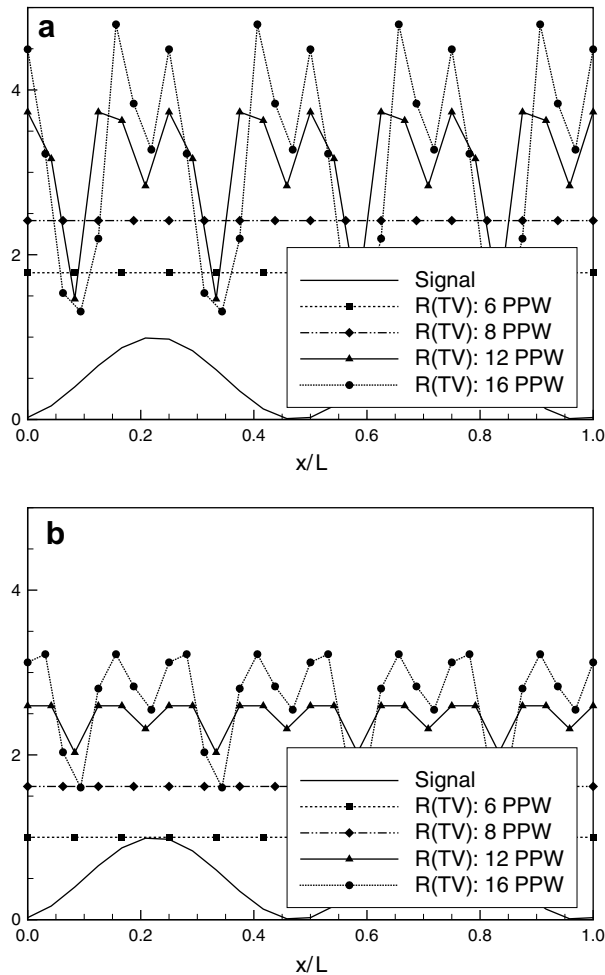

Fig. 3. (a) WENO-3. (b) WENO-4. Ratio of maximum to minimum total variation over WENO candidate stencils for a smooth sinusoidal function on grids providing varying points per wavelength (PPW).

As formulated in this section, the relative smoothness and total variation limiters generate sharp rather than smooth numerical stencil transitions. Though smooth "switches" often yield superior performance, we find that this is not true for the relative limiting procedures. A blended-stencil approach, which introduces additional computational complexity, provides results that are materially identical.

4. Numerical simulations

4.1. Shu–Osher problem

The Shu–Osher problem places smooth density fluctuations upstream of a moving shock front to probe the ability of a shock-capturing method to resolve discontinuities embedded within pseudoturbulence without damaging fine structures. Our simulations set conditions at the right boundary to be atmospheric with zero velocity and conditions at the left boundary such that the shock between the two states experiences a relative incoming Mach number of three. Sinusoidal density fluctuations are imposed upstream of this shock with wavelength $\lambda = \frac{1}{8}L$ and excursions of $\pm 0.2\rho_R$, in which the subscript R indicates the right boundary. Initially, the shock is positioned at $x/L = \lambda$, and we evolve simulations in time until $t = 0.21L/a_R$. For orientation purposes, Fig. 4 displays converged density profiles for the initial and terminal states as computed by the WENO-4 scheme on an excessively fine grid of 2048 points.

Fig. 5 presents the effects of the relative smoothness and relative total variation limiters on solutions to the Shu–Osher problem as computed by WENO-3 schemes on 192 grid points. In Fig. 5a, we plot profiles of the normalized nonlinearity index NI' for the original scheme and the two modified ones alongside a sketch of the converged density profile for reference. All indicate that neither limiter hinders adaptation where required: across the main shock and the multiple shocklets within the low-frequency region on the left. In between these shocklets and within the smooth high-frequency region in the middle, where adaptation is not necessary, NI' is noticeably lower for schemes with the limiters than for those without. Additionally, the total variation limiter outperforms the smoothness limiter in this respect. Such closer conformance to the optimal stencil should result in decreased dissipation, and this expectation is borne out in Fig. 5b, which compares each of the coarse-grid density profiles to the converged solution. In the high-frequency region, the original WENO-3 scheme is excessively damped, but the addition of either of the limiters allows most of these peaks to reach their proper amplitudes. An exception is the leftmost peak, the profile of which the smoothness limiter fails to improve and the total variation limiter improves only moderately. Finally, one small strike against the total variation limiter is that it appears to amplify a previously existing artificial excursion on the far left of the density profile.
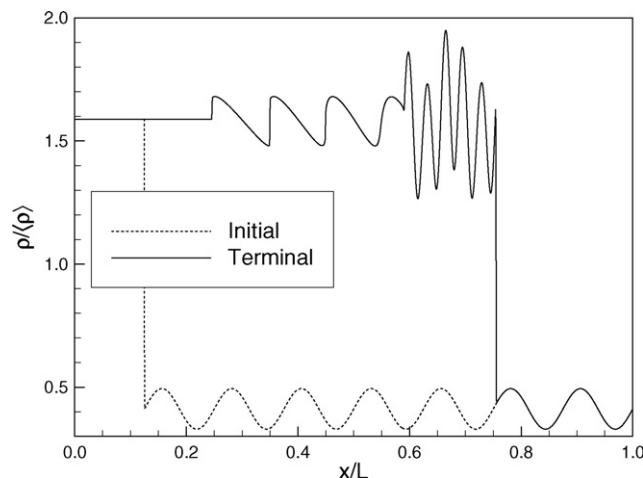

Fig. 4. Converged density profiles of the Shu-Osher problem as computed on 2048 grid points by the WENO-4 scheme.
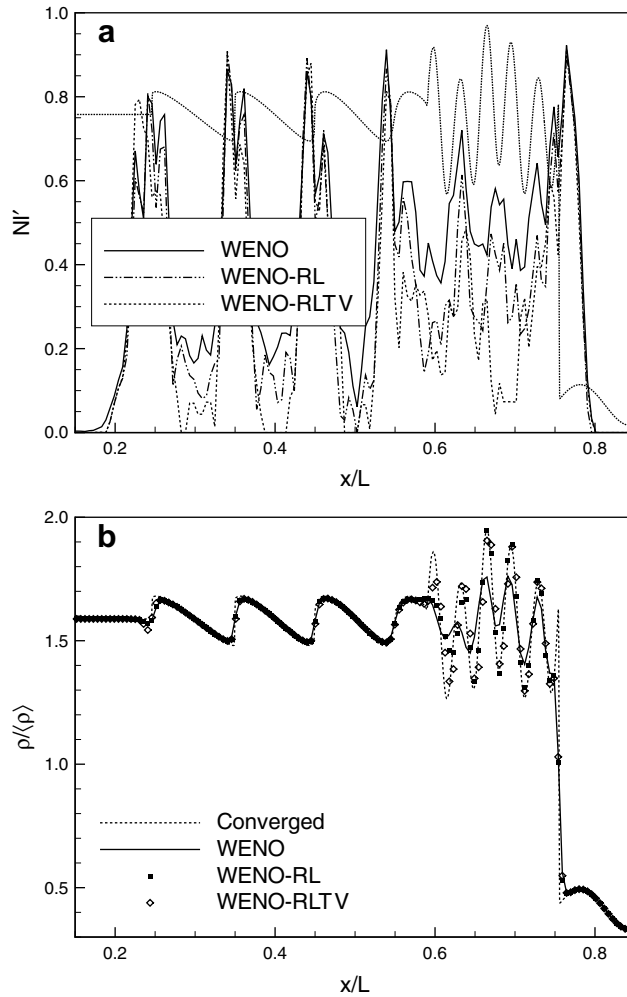
Fig. 5. (a) Profiles of normalized nonlinearity index NI′. (b) Density profiles. Shu-Osher problem as computed on 192 grid points by WENO-3 schemes employing no limiters, the relative smoothness limiter (RL), and the relative total variation limiter (RLTV).

Fig. 6 shifts attention to the corresponding WENO-4 schemes. As before, Fig. 6a displays NI′ for the original scheme, the scheme supplemented by the smoothness limiter, and the one supplemented by the total variation limiter; and we observe similar trends. Neither limiter hinders adaptation where required, across the main shock and shocklets, and in between the shocklets and within the high-frequency region, where adaptation is not necessary, NI′ is noticeably lower for schemes with the limiters, especially the total variation limiter, than for those without. Also like before, the density profiles of Fig. 6b confirm that the reduction in NI′ when limiters are employed corresponds to decreased dissipation in the high-frequency region, this time with no exceptions. Unlike before, the total variation limiter leads to small overshoots at many of these peaks, but it does not, on the other hand, seem to amplify the artificial excursion on the far left.

4.2. Compressible isotropic turbulence

Decaying three-dimensional isotropic turbulence is a canonical flow field that realistically represents the small scales of many turbulent flows and, if compressible, can generate shocklets that are strong and numerous enough to require shock-capturing methods. Its physical domain is a three-dimensional cube with periodic boundary conditions and an edge length that encompasses a sufficient sample of large-scale turbulence
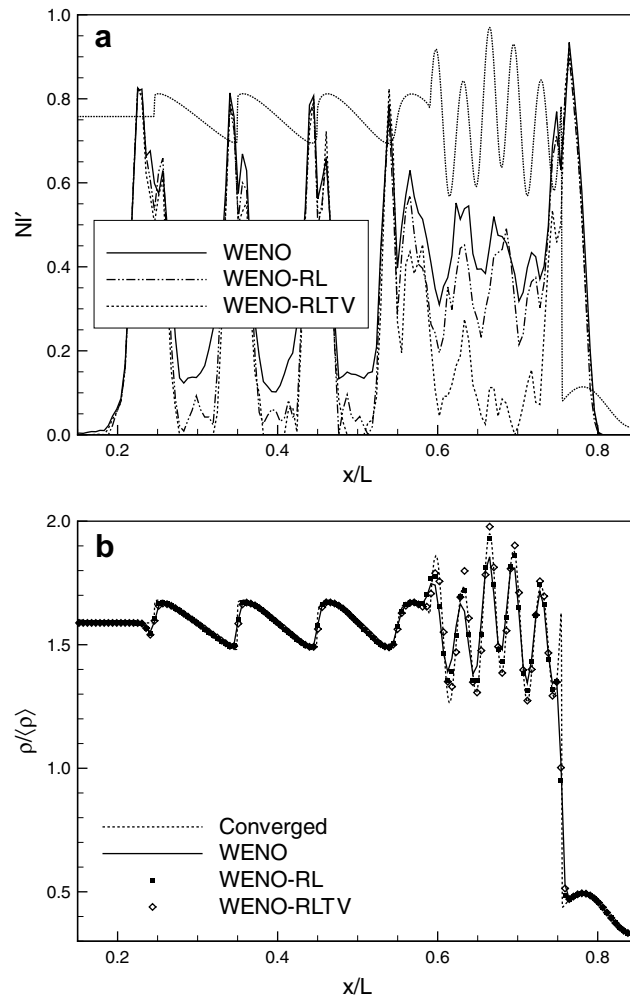
Fig. 6. (a) Profiles of normalized nonlinearity index NI′. (b) Density profiles. Shu-Osher problem as computed on 192 grid points by WENO-4 schemes employing no limiters, the relative smoothness limiter (RL), and the relative total variation limiter (RLTV).

structures; an evenly-spaced Cartesian grid discretizes this domain into N^3 points. We conduct direct numerical simulations (DNS) of isotropic turbulence that approximate the convective terms of the Navier–Stokes equations with various WENO methods, the viscous terms with fourth-order-accurate finite differences, and time advancement with a third-order-accurate low-storage Runge–Kutta scheme.

The following two nondimensional parameters are important for characterizing the state of isotropic turbulence: the Reynolds number based on the Taylor microscale

$$Re_\lambda = \frac{\langle\rho\rangle u'_{\text{rms}}\lambda}{\langle\mu\rangle} \tag{18}$$

in which u'_{rms} is the root-mean-squared velocity (per component) and λ is the Taylor microscale, and the turbulent Mach number

$$M_t = \frac{q}{\langle a\rangle} \tag{19}$$

in which $\langle a\rangle$ is the average speed of sound and q is the root-mean-squared total velocity magnitude. Note that Re_λ and M_t are not constant throughout a simulation because the global strength of the turbulent fluctuations steadily decays over time without external forcing, which we do not include. Of the multiple sets of

isotropic turbulence conditions that we have examined for this study, the case of initial $Re_\lambda = 50$ and $M_t = 0.7$ is observed to demonstrate typical results. For these conditions, we find that a converged solution can be obtained with the original WENO-4 scheme on 192^3 points and that a 96^3 grid is appropriate for active testing of the two relative limiters. The initial field is a solenoidal approximation that we evolve on 224^3 grid points for the duration of the initialization transient, which we find to be roughly $1.5\tau_t$, where τ_t is the initial state's reference time λ/u'_{rms}. We then filter the resulting field such that $N = 192$ and $N = 96$ to begin our data runs.

Fig. 7 presents the effects of the relative smoothness and relative total variation limiters on the turbulent kinetic energy ρq^2 of isotropic turbulence as computed by WENO-3 schemes. In Fig. 7a, we track the temporal evolution of average TKE normalized by its value at $t/\tau_t = 1.5$ (when the test runs begin). The converged solution indicates the rate of energy decay that is natural, and the remaining solutions, on the coarser grid, exhibit varying degrees of additional dissipation due to their numerical methods. Both the WENO-RL and the WENO-RLTV schemes, though they fall short of achieving grid-convergence, succeed in reducing excess dissipation by more than 50%, and neither meaningfully outperforms the other. Informa-
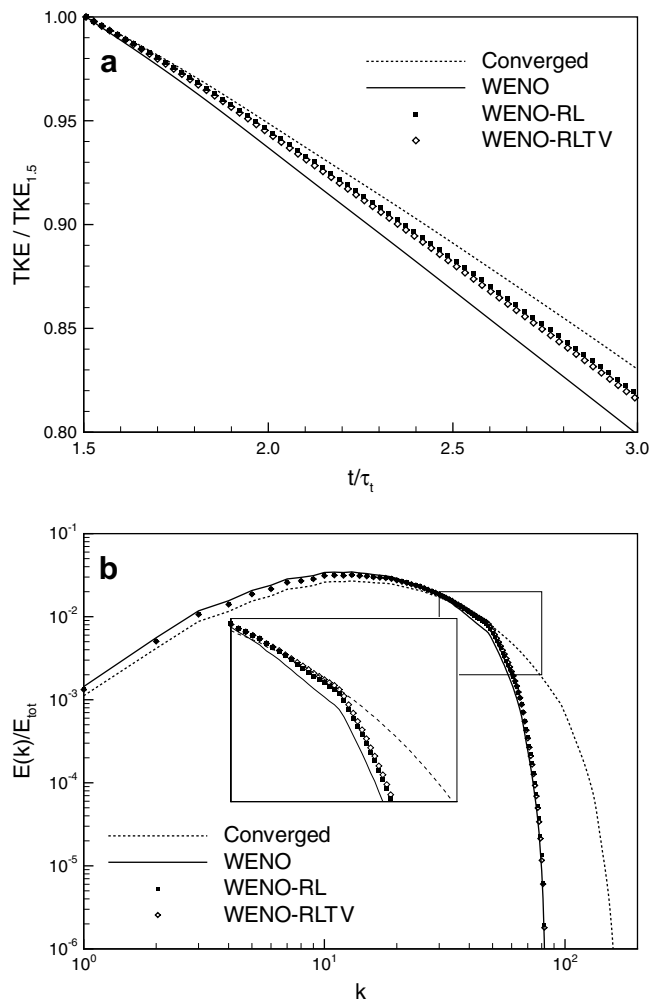

Fig. 7. (a) Temporal evolution of average TKE (normalized by its value at $t/\tau_t = 1.5$). (b) Nondimensional energy spectrum at $t/\tau_t = 3.0$. Turbulent kinetic energy of compressible isotropic turbulence as computed on 96^3 grid points by WENO-3 schemes employing no limiters, the relative smoothness limiter (RL), and the relative total variation limiter (RLTV) for initial $Re_\lambda = 50$ and $M_t = 0.7$.

tion of a more local nature is available through the instantaneous energy spectra of Fig. 7b, which displays nondimensional spectra for each of the schemes at $t/\tau_t = 3.0$. Note that the offset between the converged solution and the others at low wavenumbers is merely an artifact of the normalization. Within the zoomed area, both the WENO-RL and WENO-RLTV schemes remain attached to the converged spectrum through noticeably higher wavenumbers than the original WENO scheme, and, again, neither behaves substantially differently from the other.

The Taylor microscale λ is useful as an additional aggregate characterization of the state of an isotropic turbulence field because its dependence on the first derivative of velocity as well as velocity itself causes it to be more sensitive than global turbulent kinetic energy to local flow variations. Thus, in Fig. 8, we plot the temporal evolution of λ under conditions identical to those of Fig. 7. The sizable gap between the converged solution and the unmodified coarse-grid solution becomes significantly smaller when either of the relative limiters is employed, and here, also, neither limiter produces results that differ significantly from those of the other.

We turn now to the corresponding WENO-4 schemes – unmodified, smoothness-limited, and total-variation-limited – and proceed through an identical style of analysis. Fig. 9a tracks the decay of average turbulent kinetic energy, and, as before, both the WENO-RL and WENO-RLTV schemes succeed in reducing excess dissipation to approximately the same degree. Moreover, the reduction this time is nearly sufficient to allow these two coarse-grid schemes to be deemed grid-converged, at least by this particular measure. Recall that the original grid-converged solution required a WENO-5 method on 192^3 grid points while the current active tests use only 96^3. In the instantaneous energy spectra of Fig. 9b, we observe that, also like before, both of the relative limiters marginally extend the range of wavenumbers for which the coarse-grid solution remains attached to the converged spectrum. Now, however, the WENO-RL and WENO-RLTV schemes are no longer indistinguishable from one another; the total variation limiter leads to a slightly truer slope than the smoothness limiter. This separation is also echoed within the temporal evolution of the Taylor microscale in Fig. 10, during which the WENO-RLTV solution approaches the converged solution quite closely and more so than the WENO-RL solution.

As we mentioned previously, we have conducted such simulations and analyses for other isotropic turbulence conditions as well, specifically for combinations of initial $Re_\lambda = \{35,50,75\}$ and $M_t = \{0.4,0.7,1.0,1.3\}$. Because the qualitative trends of these results are both self-consistent and completely exemplified by the case already discussed, we do not explicitly include them.
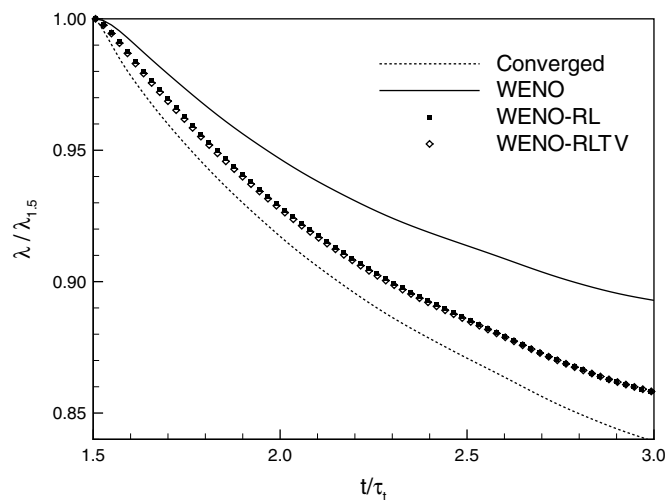

Fig. 8. Taylor microscale λ of compressible isotropic turbulence as computed on 96^3 grid points by WENO-3 schemes employing no limiters, the relative smoothness limiter (RL), and the relative total variation limiter (RLTV) for initial $Re_\lambda = 50$ and $M_t = 0.7$.
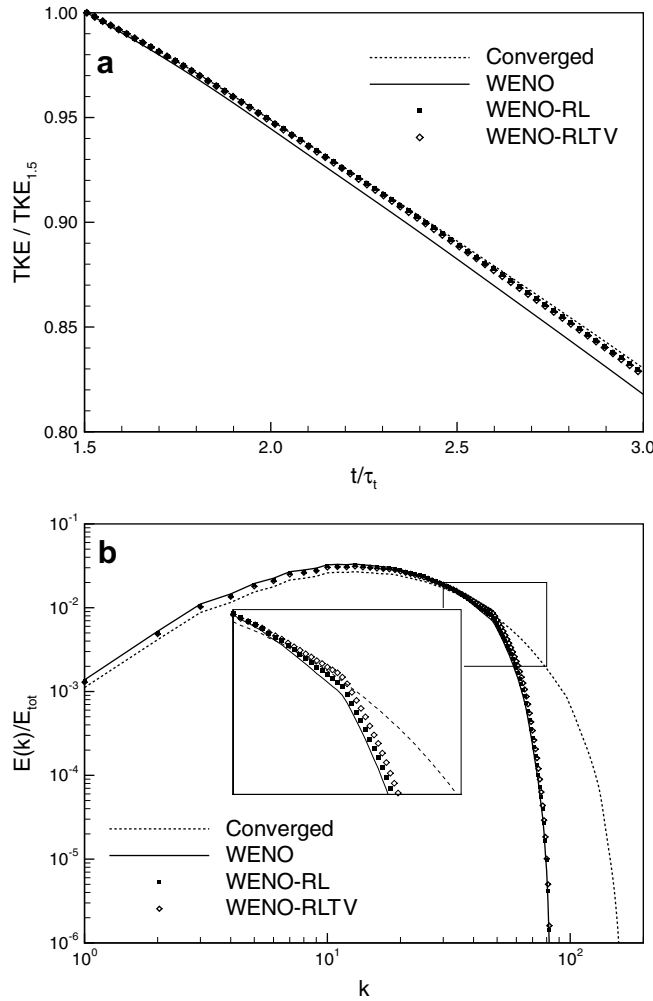
Fig. 9. (a) Temporal evolution of average TKE (normalized by its value at $t/\tau_t = 1.5$). (b) Nondimensional energy spectrum at $t/\tau_t = 3.0$. Turbulent kinetic energy of compressible isotropic turbulence as computed on 96^3 grid points by WENO-4 schemes employing no limiters, the relative smoothness limiter (RL), and the relative total variation limiter (RLTV) for initial $Re_\lambda = 50$ and $M_t = 0.7$.

4.3. Computational performance

In Table 1, we quantitatively summarize the increase in computational expense incurred and the decrease in numerical error achieved by each of the modified WENO schemes that we have discussed in this section. For the Shu–Osher problem, we define the aggregate error to be the root-mean-square difference between the density profile of the converged solution and the profile generated by the tested scheme. For compressible isotropic turbulence, we define it to be the root-mean-square difference between the converged solution's natural decay of average turbulent kinetic energy and the decay produced by the tested scheme. Because the former is of a more local nature than the latter and therefore more sensitive to the precise resolution of fine structures, it is not surprising that the smoothness and total variation limiters are more successful, by these measures, in isotropic turbulence. Overall, the two relative limiters add less than one-fifth to computational expense but reduce numerical dissipation roughly one-quarter in the Shu–Osher problem and roughly three-quarters in isotropic turbulence. The extra quantity TV_k in Eq. (15) that the total variation limiter must compute across each of the r candidate stencils is what causes its expense to be greater than the smoothness limiter's; but since the cost of this calculation rises more slowly with r than the cost of core WENO computations, its relative efficiency improves with increasing r.
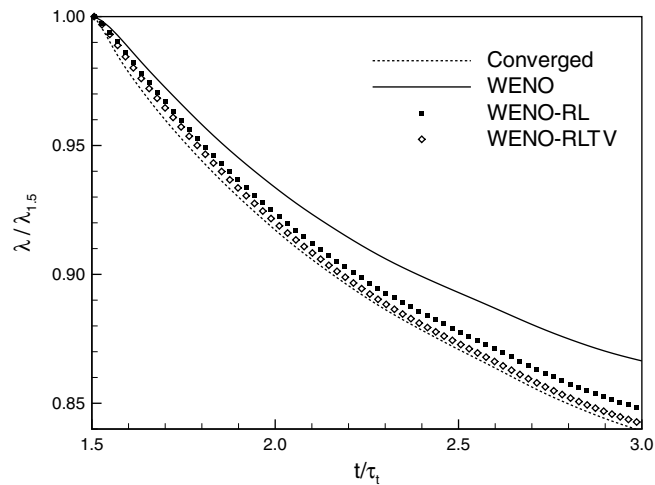
Fig. 10. Taylor microscale λ of compressible isotropic turbulence as computed on 96^3 grid points by WENO-4 schemes employing no limiters, the relative smoothness limiter (RL), and the relative total variation limiter (RLTV) for initial $Re_\lambda = 50$ and $M_t = 0.7$.

Table 1
Quantified computational performance of the relative smoothness limiter (RL) and relative total variation limiter (RLTV) for 3- and 4-point WENO schemes

	WENO-RL		WENO-RLTV	
	WENO-3 (%)	WENO-4 (%)	WENO-3 (%)	WENO-4 (%)
Computational time	+4	+4	+20	+10
Shu–Osher problem error	−23	−21	−24	−27
Isotropic turbulence error	−65	−77	−56	−82

5. Conclusions

The adaptation mechanism of the WENO methodology is overly sensitive to moderate flow field variations that do not require shock-capturing. To alleviate this deficiency, we have appended the standard definition of candidate stencil smoothness such that unnecessary adaptation is largely suppressed. The resulting push toward greater reliance on the linear optimal stencil translates, in theory and in practice, into markedly decreased numerical dissipation from nonlinear sources and improved grid-convergence properties. Though a previously proposed absolute smoothness limiter can also accomplish this, the appropriate threshold value for that limiter is both scheme- and problem-dependent. In contrast, the relative smoothness and total variation limiters that we have developed are found to be broadly effective without the need for costly parameter tuning. Based on the behavior of the original smoothness measurement along discretized smooth data, we have determined that appropriate universal threshold values for Eqs. (13) and (17) are, respectively, $\alpha_{RL} = 10$ and $\alpha_{RL}^{TV} = 5$.

Performance characteristics of these WENO-RL and WENO-RLTV schemes have been presented for direct numerical simulations of the Shu–Osher problem and compressible isotropic turbulence. In the Shu–Osher problem, both of the relative limiters verifiably discouraged unnecessary adaptation across high-frequency smooth oscillations and, as a result, significantly enhanced numerical accuracy. Though the total variation limiter sometimes appeared less stable than the smoothness limiter, discrepancies were minor and did not grow with time. In isotropic turbulence, the two limiters successfully reduced the excess decay of turbulent kinetic energy that stems from numerical dissipation, and in the case of the WENO-4 scheme, they did so to the point of allowing grid-convergence to be attained with 96^3 grid points instead of 192^3. Additionally, the energy spectrum and Taylor microscale evolution of the WENO-4 case indicated a slight superiority of the total variation limiter over the smoothness limiter (although this advantage shrinks when the former's addi-

tional computational expense is considered). Overall, the gains in numerical accuracy made possible by each of the relative limiters justify their computational costs.

Therefore we support and encourage the adoption of either the relative smoothness limiter or the relative total variation limiter into the linearly bandwidth-optimized WENO methodology as a means of mitigating nonlinear numerical dissipation. We particularly favor 4-point WENO schemes that have been so modified.

Acknowledgements

References

[1] X.-D. Liu, S. Osher, T. Chan, Weighted essentially non-oscillatory schemes, Journal of Computational Physics 115 (1) (1994) 200–212.
[2] G.-S. Jiang, C.-W. Shu, Efficient implementation of weighted ENO schemes, Journal of Computational Physics 126 (1) (1996) 202–228.
[3] E. Garnier, M. Mossi, P. Sagaut, P. Comte, M. Deville, On the use of shock-capturing schemes for large-eddy simulations, Journal of Computational Physics 153 (1) (1999) 273–311.
[4] V.G. Weirs, A numerical method for the direct simulation of compressible turbulence, Ph.D. thesis, University of Minnesota, December 1998.
[5] M.P. Martín, E.M. Taylor, M. Wu, V.G. Weirs, A bandwidth-optimized WENO scheme for the direct numerical simulation of compressible turbulence, Journal of Computational Physics 220 (1) (2006) 270–289.
[6] M.P. Martín, Shock-capturing and the LES of high-speed flows, in: Annual Research Briefs, Center for Turbulence Research, 2000, pp. 193–198.
[7] M. Wu, E.M. Taylor, M.P. Martín, Assessment of STBLI DNS data and comparison against experiments, AIAA Paper No. 2005–4895, American Institute of Aeronautics and Astronautics, 2005.
[8] Z.J. Wang, R.F. Chen, Optimized weighted essentially nonoscillatory schemes for linear waves with discontinuity, Journal of Computational Physics 174 (1) (2001) 381–404.
[9] A.K. Henrick, T.D. Aslam, J.M. Powers, Mapped weighted essentially non-oscillatory schemes: Achieving optimal order near critical points, Journal of Computational Physics 207 (2) (2005) 542–567.